Research Article

Cancer Epidemiology, Biomarkers & Prevention

Potential Markers from Serum-Purified Exosomes for Detecting Oral Squamous Cell Carcinoma Metastasis

Cuiping Li[1], Yang Zhou[2], Junjun Liu[3], Xiaoping Su[1], Hao Qin[3], Suhua Huang[1], Xuanping Huang[1,3], and Nuo Zhou[1,3]

Abstract

Background: Blood contains exosomes that are related to tumor cells. Those exosomes can regulate communication between cells and have a great influence on a variety of tumor-associated proceedings through their target cells. Therefore, serum exosomes (SE) were supposed to play a crucial role in cancer development.

Methods: This study presented a quantitative proteomics analysis to identify the protein content in SEs including 30 subjects from oral squamous cell carcinoma (OSCC) patients with lymph node metastasis (LNM), OSCC patients with no LNM (NLNM), and healthy controls (HC). Differentially expressed proteins (DEP) were analyzed by bioinformatics, and then a total of 30 subjects were used for Western blot and 60 subjects for IHC, ELISA, and RT-PCR verifications. The correlations were assessed between DEP expression and clinicopathologic factors.

Results: A total of 415 proteins were identified. Comparing with HC and OSCC-NLNM, we found 37 proteins and 28 proteins in the SEs of OSCC-LNM, respectively. There were significant correlations among the expression of PF4V1 with tumor differentiation level, PF4V1 and F13A1 with the number of positive nodes, and ApoA1 with smoking and drinking. ROC curve analysis indicated that the combinations of the different biomarkers or specimen were obviously superior to single biomarker or specimen for diagnosing OSCC-LNM.

Conclusions: We conclude that PF4V1, CXCL7, F13A1, and ApoA1 from SEs may be related to the metastasis of OSCC, which would be helpful in the diagnosis of OSCC-LNM.

Impact: Biomarkers from SEs could help with the diagnosis of metastasis in OSCC.

Introduction

Oral cancer is a type of head and neck cancer, and the location of oral cancer occurrence includes the lip, tongue, floor of mouth, buccal, gingiva, and palate (1). Oral cancer is the sixth most common cancer diagnosed worldwide and causes more than 145,000 deaths annually; it is also the sixth most common cause of cancer death, especially for men who drink alcohol and smoke. More than 90% of oral cancers are oral squamous cell carcinomas (OSCC), and more than 50% of OSCCs have a high rate of lymph node metastasis (LNM; ref. 2). Once patients are diagnosed with OSCC with LNM, their 5-year survival rate will fall from 80% to less than 40% (3). Therefore, it is important to understand the mechanisms behind the metastasis that is a leading cause in most deaths of OSCC patients and poses a major challenge in the early detection and timely treatment of OSCC with LNM. As one of the 10 hallmarks of cancer, the activation of tumor invasion and metastasis is a complex and critical multistep process (4, 5). Consequently, there is an area of intense research on the molecular pathogenesis behind the development of such metastatic advances and specific markers that can be used to screen for metastasis in LNM patients rapidly, noninvasively, and with high sensitivity. Recent studies have found that extracellular vesicles called exosomes played an important role in explaining metastasis (6).

Exosomes are small, spherical bilayered membrane vesicles, with an average diameter of 30 to 100 nm, and are secreted from all kinds of cells, including tumor cells, in a range of biological fluids, including plasma, saliva, urine, blood, cerebrospinal fluid, and cell culture media (6–8). An intercellular communication system consists of these vesicles, meaning that exosomes are potentially valuable for biomarker selections as well as disease therapies, such as cancer therapies. Exosomes involve a variety of proteins and bioactive lipids, and exosome compositions change with the specific donor cell type. The protein members of exosomes include the transmembrane 4 superfamily (CD9, CD63, and CD81) and tumor susceptibility gene 101 (TSG101; ref. 9). There is still not a complete understanding of the functional

[1]Guangxi Key Laboratory of the Rehabilitation and Reconstruction of Oral and Maxillofacial Research; Guangxi Key Laboratory of Oral and Maxillofacial Surgery Disease Treatment; Guangxi Clinical Research Center for Craniofacial Deformity, College of Stomatology, Guangxi Medical University, Nanning, P.R. China. [2]School of Information and Management, Guangxi Medical University, Nanning, P.R. China. [3]Department of Oral and Maxillofacial Surgery, the Affiliated Stomatology Hospital of Guangxi Medical University, Nanning, P.R. China.

Note: Supplementary data for this article are available at Cancer Epidemiology, Biomarkers & Prevention Online (http://cebp.aacrjournals.org/).

C. Li, Y. Zhou, and J. Liu contributed equally to this article.

Corresponding Authors: Nuo Zhou, the Affiliated Stomatology Hospital of Guangxi Medical University, Nanning 530021, P.R. China. Phone: 086-771-2705693; Fax: 086-771-2705693; E-mail: gxzhounuo@sina.cn; and Xuanping Huang, hxp120@126.com

Cancer Epidemiol Biomarkers Prev 2019;XX:XX–XX

doi: 10.1158/1055-9965.EPI-18-1122

characteristics of exosomes (10). A new study indicated that tumor-derived exosomes could recruit bone marrow–derived cells to the premetastatic niche, which is similar to the functions of cytokines and soluble factors, thereby contributing to the production of a permissive microenvironment for tumor metastases and spreading by transferring oncoproteins (11). Furthermore, tumor-derived exosomes mediate vascular leakiness, which have become a crucial feature of premetastatic niche formation (12, 13). Exosomes are not just simple cellular debris. They act as extracellular organelles that play local or distinct roles in cell–cell communication while promoting the motility of recipient cells to proliferate and remodel the extracellular matrix (ECM) that supports the proliferation and migration of tumor (14). Tumor cell–derived exosomes manifest multiple sites of action. Some recent studies confirmed that the tumor cell–derived exosomes could induce apoptosis of tumor cells and enhance antitumor immunity (15, 16). However, other studies indicated that tumor cell–derived exosomes may promote tumor progression by exhibiting immunosuppressive properties, facilitating tumor invasion and metastasis, stimulating tumor cell proliferation, and inducing drug resistance (17–22). Therefore, exosomes are closely associated with tumor development and could serve as markers and novel therapeutic targets for early prognostic and treatment benefit. Up to now, no study has focused on differentially expressed proteins (DEP) of exosomes purified from serum of OSCC patients, especially OSCC-LNM patients.

In this study, we applied proteomic and bioinformatic strategies to determine the biological functions of serum exosomes (SE) derived from OSCC-LNM. The proteome profiles of SEs from OSCC-LNM patients, OSCC-NLNM patients, and healthy controls (HC) were compared using a combination of LC-MS/MS analyses. Identified DEPs might be associated with tumor cell growth and adhesion. This study provides the first evidence that an initial relationship between the proteins of SEs and OSCC-LNM patients may be useful in both the early evaluation of OSCC-LNM and the development of novel diagnostics and therapeutics.

Materials and Methods

Study subjects and sample collections

Patients diagnosed with primary OSCC in the Affiliated Stomatology Hospital of Guangxi Medical University (ASHGMU, Nanning, China) and HCs from the Guangxi Medical University First Affiliated Hospital were recruited to this study from May 2017 to January 2018. All samples from patients who were from 25 to 75 years old and without diabetes, blood diseases, or other tumors were collected before primary tumor resection at ASHGMU, apart from obtainment of tissue samples during surgery. None of the patients received chemotherapy or radiotherapy before sample collection. We also obtained samples from HCs who had no evidence of disease. They ranged from 25 to 75 years old and also underwent a full diagnostic assessment to exclude diabetes, blood diseases, or tumors. We distributed OSCC patients into two groups: those with LNM without extranodal extension or lymphovascular invasion and those with NLNM. Informed consent was obtained from all study subjects. The ethics committee of Guangxi Medical University approved the study.

Serum and SE samples from a total of 30 subjects were used for screening test and Western blotting verification. Subject demographics were as follows: Male/female ratio was 7/3, 8/2, and 7/3 for OSCC with LNM, OSCC with NLNM, and HC groups, respectively; the average age was 43.5, 43.8, and 44.2 for OSCC with LNM, OSCC with NLNM, and HC groups, respectively. Serum and whole blood from a total of 60 subjects were used for RT-PCR and ELISA verification from serum and SEs, and the subject demographics were as follows: For the OSCC with LNM group, the male/female ratio was 12/8, and the average age was 44.6; for the OSCC with NLNM group, the male/female ratio was 12/8, and the average age was 44.2; for the HC group, the male/female ratio was 13/7, and the average age was 44.9. A total of 60 pairs of cancerous tissues and their corresponding adjacent tissues were used for RT-PCR and IHC verification. The demographics of the patients who provided the tissues were as follows: For the OSCC group, the male/female ratio was 33/27, and the average age was 45.6; for the OSCC with LNM group, the male/female ratio was 17/13, and the average age was 45.3; and for the OSCC with NLNM group, the male/female ratio was 16/14, and the average age was 44.9. The age and sex were matched between all case groups and control groups. The whole experimental workflow was shown in Supplementary Fig. S1.

Isolation and identification of SEs

The exosomes of 500 μL serum from each sample were isolated according to the instructions from the manufacturer (SBI System Biosciences). The pellet from every 500 μL serum was resuspended in 500 μL of PBS. The samples were fixed with 3% glutaraldehyde for 3 hours, and soaked and rinsed three times in 0.1 mmol/L sodium cacodylate buffer at room temperature. The samples were fixed with osmium tetroxide for 1 hour and soaked and rinsed in 0.1 mmol/L sodium cacodylate buffer. A Hitachi S7650 scanning electron microscope visualized the exosomes after samples were dried, mounted on specimen stubs, and sputter coated. We also characterized the amount and size of exosomes to confirm this information using nanosight analysis with Flow NanoAnalyzer (NanoFCM Inc.). Western blotting was utilized to identify the marker proteins of exosomes. Fifty micrograms of the protein was used for Western blotting and was then separated on a 12% SDS-PAGE gel and transferred to membranes (Millipore). Membranes were blocked and then incubated overnight with rabbit anti-CD9 (1:1,000, Santa Cruz Biotechnology), rabbit anti-CD63 (1:1,000, Santa Cruz Biotechnology), rabbit anti-HSP70 (1:1,000, Abcam), or rabbit anti-GAPDH (1:5,000, Abcam). The secondary antibody was anti-rabbit IgG (1:2,000, Sino Biological Inc.). A chemiluminescent gel imaging system (FluorChem HD2; ProteinSimple) scanned the bands. A fraction of the resuspended exosomes was lysed using Radio Immunoprecipitation Assay buffer, and then the total protein concentration was detected using a BCA protein assay kit.

Label-free quantitative MS and bioinformatic analysis

Samples were processed and then analyzed for LC-MS. All analyses were performed using a QExactive plus Orbitrap mass spectrometer (Thermo Fisher Scientific) equipped with a nanoelectrospray ion source. All samples after enzymolysis were dissolved in 0.1% formic acid in water (buffer A), and 0.1% formic acid Acetonitrile in water (84% Acetonitrile, buffer B). Peptides were desalted and then separated by Zorbax 300SB-C18 peptide traps (Agilent Technologies) and reversed-phase liquid chromatography (Column Technology Inc.). We operated the survey

mass spectrometer with the following settings: Scanning range of positive ion was 300 to 2,000 m/z; the survey mass spectrum with a resolving power was 60,000; AGC target was 1.0×10^{-6}; the survey Maximum IT was 50 ms; the number of scan ranges was 1; and dynamic exclusion was 30.0 s. The quality charge of polypeptides and their fragments were collected with the following methods: MS2 Activation Type: CID; Isolation window: 1 m/z; the secondary mass spectrum with a resolving power: 15,000 at m/z 200; Microscans: 1; Maximum IT: 150 ms; AGC target: 5×10^4; Normalized collision energy: 35eV; and Underfill ratio: 0.1%. The raw data were analyzed by Maxquant software and UniProt Homo sapiens (Version 1.4.1.1). The search parameters were as follows: (1) Up to 2 leakage points were allowed; (2) fixed modification was carbamidomethylation; and (3) dynamic modifications were oxidation and acetyl.

The identified (score > 0) proteins were next clustered into Gene Ontology (GO) and categories to identify the OSCC-LNM–related physiologic processes implicated by the exosomal proteins using bioinformatic tools. The UniProt online ID mapping server was applied to convert UniProtKB accessions into Entrez Gene IDs in GO analysis, which were subjected to FunRich software 2.1.221. GO included biological processes, molecular functions, and cellular components, and the terms of the charts were acquired by applying default statistical parameters (threshold: count 2, ease 0.1).

Protein class analysis was performed with the Panther classification system, which was conducted by applying the WEB-based GEne SeT AnaLysis Toolkit (http://bioinfo.vanderbilt.edu/webgestalt/) in Kyoto Encyclopedia of Genes and Genomes (KEGG) pathway. For pathways, the statistical significance was on the base of a P value of less than 0.05 and the appearance of at least two target genes.

The threshold of DEPs was 1.5-fold change (>1.5 or <0.067) for both up- and downregulation of expression in the comparison of case group/control group.

ELISA, Western blot, IHC, and RT-PCR verification

To verify the proteomics results, ELISA and Western blot verification were exercised to test the expression levels of identified proteins from SEs and serum. Based on the bioinformatics analysis, four proteins including platelet factor 4 variant (PF4V1), Apolipoprotein A-I (ApoA1), C-X-C motif chemokine (CXCL7), and coagulation factor XIII, A1 (F13A1) were chosen for validation. PF4V1 was derived from CXC chemokine 4 (CXCL4), which was also chosen for validation in this study. The protein concentrations of CXCL7 were measured by the ELISA kit (ab100613, Abcam). The protein concentrations of CXCL4 and ApoA1 were measured by a different ELISA kit (Neobioscience). There were no suitable commercial kits for F13A1 and PF4V1. Mouse anti-F13A1 (1:500 for Western blot/1:50 for IHC, ab1834, Abcam), rabbit anti-PF4V1 (1:1,000 for Western blot/1:200 for IHC, Sigma), rabbit anti-CXCL7 (1:1,000 for Western blot/1:200 for IHC, Sigma), and GAPDH (1:2,000, Sino Biological Inc.) antibodies were applied in Western blot and IHC verification. Goat serum (ZSGB-BIO) used for secondary antibodies was applied in IHC verification, respectively.

We also conducted RT-PCR verification. Expression levels of *PF4V1*, *CXCL4*, *CXCL7*, *ApoA1*, and *F13A1* mRNA in tissue, serum, and whole blood were quantitated using RT-PCR. Total RNA was extracted and purified using RNeasy spin columns, which was then reverse transcribed into cDNA following the manufacturer's specifications (Takara). Quantification of mRNA expression was performed using the SYBR Green qRT-PCR Kit (Takara) on an ABI StepOne/StepOnePlus Detection System (Applied Biosystems). Conditions for PCR were 95 degrees for 15 seconds and 68 degrees for 2 minutes for 40 cycles. The amplified products were normalized using GAPDH as an internal control, and the values of gene expression were computed as fold change in relation to GAPDH by using the $2^{-\Delta\Delta Ct}$ or $2^{-\Delta Ct}$ method (23, 24). The primer information is shown in Supplementary Table S1.

Clinicopathologic data analysis of DEPs and statistical analysis

Relevant clinical details and basic characteristics were collected when the patients consented to clinical examination. The correlation was analyzed with statistic methods between different clinicopathologic factors and DEP expression by using χ^2 test, McNemar, and Fisher exact tests from SPSS 20.0 software package. The confounders were eliminated by using regression multivariate modeling. The clinicopathologic factors included gender (male/female), nationality (Han nationality/Zhuang nationality), tumor stage (I/II stage/III/IV stage), tumor differentiation degree (high differentiated squamous cell carcinoma/low differentiated squamous cell carcinoma), smoking state (smoking/no smoking), and drinking state (drinking/no drinking). A more detailed assessment was conducted to investigate DEP expression in the six grades of age brackets, including 20 to 40 years, 41 to 50 years, 51 to 60 years, 60 to 80 years, $\leq$50 years, and >50 years, and the number of positive nodes of OSCC-LNM, including 1 positive node, 2 to 4 positive nodes, $\geq$5 positive nodes, $\geq$2 positive nodes, <5 positive nodes in tissue, 1 to 2 positive nodes, 4 to 5 positive nodes in serum and $\geq$5 positive nodes, and <5 positive nodes in SEs. Gene Expression Profiling Interactive Analysis (GEPIA), a Web server for cancer and normal gene expression profiling and interactive analyses, was used to evaluate the connection between *ApoA1*, *CXCL7*, *PF4V1*, *F13A1*, and the overall survival of head and neck squamous cell carcinoma.

Establishment of diagnostic models

The statistically significant findings from the verification analyses were used to establish various diagnostic models to have further insight into the utility of these four candidate biomarkers. ROC curves and the AUC were calculated to analyze the specificity and sensitivity in the comparisons of single-candidate biomarkers and their combinations (25). The statistical analyses were performed using a binary logistic regression analysis in SPSS 20.0 software package (26). Data analyses were conducted from triplicate experiments. Results are shown as mean $\pm$ SD. Statistically significant differences were analyzed by the Student t test and nonparametric test ($P < 0.05$) using the SPSS 20.0 software package.

Results

Extraction and identification of SEs

The integrity morphologic images of SEs are displayed in the electron micrographs (Fig. 1A–C). The specific exosome markers of CD9, CD63, and HSP70 were also detected in Western blot test (Fig. 1D). The particle size distribution maps

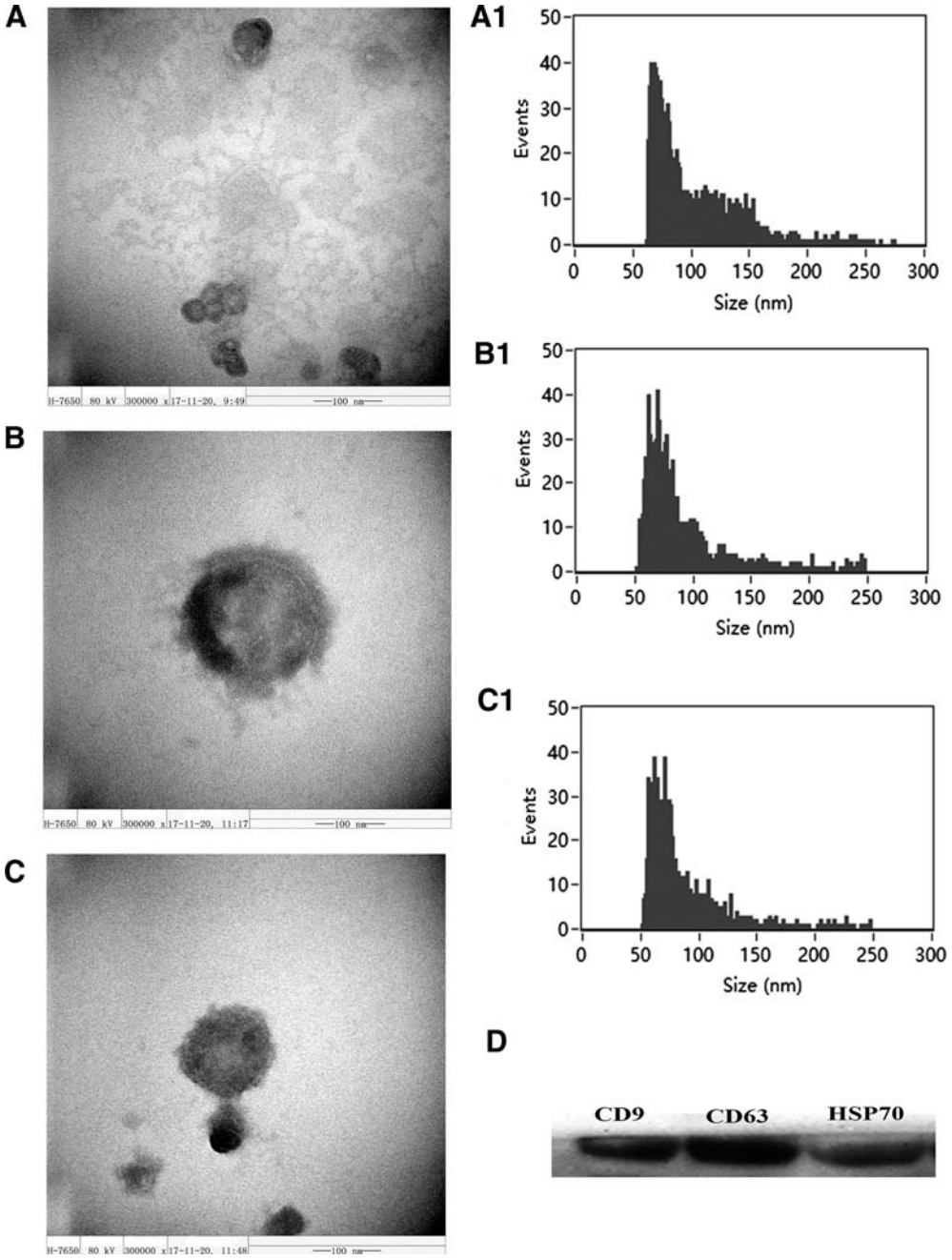

Figure 1.
The characterization of SEs. The pictures of transmission electron microscopy (**A**) and nanosight analysis with Flow NanoAnalyzer (**A1**) of SEs preprocessed from the HC group. The pictures of transmission electron microscopy (**B**) and nanosight analysis with Flow NanoAnalyzer (**B1**) of SEs preprocessed from the OSCC with LNM group. The pictures of transmission electron microscopy (**C**) and nanosight analysis with Flow NanoAnalyzer (**C1**) of SEs preprocessed from the OSCC with NLNM group. **D,** SE markers identified by Western blotting.

of SEs are shown in Fig. 1A1–C1. The particle size and density of SEs from the HC group, LNM group, and NLNM group were 99.49 ± 36.50 nm, 86.76 ± 33.96 nm, 83.56 ± 31.71 nm and 1.51×10^{10} particles/mL, 1.44×10^{10} particles/mL, and 1.24×10^{10} particles/mL, respectively. An average diameter of SEs from the HC group, LNM group, and NLNM group was 50 to 250 nm.

Quantitative proteomics and bioinformatic analysis

A total of 415 proteins were identified including 252 proteins for OSCC-LNM when compared with HC, 255 proteins for OSCC-LNM when compared with OSCC-NLNM, and 257 proteins for OSCC-NLNM when compared with HC. According to the inclusion criteria of the DEPs, a total of 37 DEPs with 20 upregulated proteins and 17 downregulated proteins were

Table 1. Comparison of DEPs identified in SEs of the OSCC-LNM group versus the HC group

Number	Accession number	Abbreviation	Full name	Molecular weight (kDa)	Sequence length	*Q* value[a]	Score[b]	OSCC-LNM/HC	*P* value	Expression
1	sp|P04275|	VWF	von Willebrand factor	309.26	2813	0	157.03	3.4326479	0.005	↑
2	tr|D3DP13|	FGB	Fibrinogen beta chain, isoform CRA_e	39.736	344	0	100.2	3.1698038	0.008	↑
3	tr|B4E1I8|	LRG1	cDNA FLJ54228, highly similar to leucine-rich alpha-2-glycoprotein	36.494	330	0	56.239	2.8420843	0.029	↑
4	tr|Q6LAM1|	CFI	Heavy chain of factor I (fragment)	35.883	321	0	31.891	2.4030773	0.002	↑
5	tr|A2J1M2|	ENSG00000223931	Rheumatoid factor RF-IP9 (fragment)	10.549	98	0	30.441	2.2035086	0.028	↑
6	sp|P02671|	FGA	Fibrinogen alpha chain	94.972	866	0	88.917	2.0509267	0.006	↑
7	tr|A0A125QYY9|	ENSG00000223931	IBM-B2 heavy-chain variable region (fragment)	13.569	123	0	98.895	1.8935852	0.003	↑
8	tr|A0A0F7SYK7|	ENSG00000223931	IGHV1-46 protein (fragment)	10.173	91	0	15.422	1.8274823	0.027	↑
9	tr|A0A024RAA7|	C1QC	Complement component 1, q subcomponent, C chain, isoform CRA_a	25.773	245	0	94.934	1.8169817	0.003	↑
10	tr|V9GYE7|	CFHR2	Complement factor H-related protein 2	28.912	254	0	24.488	1.6460515	0.002	↑
11	tr|A8K2T4|	C7	cDNA FLJ78207, highly similar to human complement protein component C7 mRNA	93.406	843	0	323.31	1.6075309	0.040	↑
12	sp|Q06033|	ITIH3	Inter-alpha-trypsin inhibitor heavy-chain H3	99.848	890	0	82.334	1.5961385	0.019	↑
13	tr|Q6N091|	ENSG00000223931	Uncharacterized protein DKFZp686C02220 (fragment)	54.159	500	0	63.267	1.5460653	0.030	↑
14	tr|A0A0 × 9UWK7|	ENSG00000223931	MS-D4 heavy-chain variable region (fragment)	13.525	122	0	76.321	1.5418579	0.035	↑
15	tr|A8K008|	ENSG00000223931	Uncharacterized protein	51.596	472	0	62.743	1.5019136	0.016	↑
16	sp|P10909|	CLU	Clusterin	52.494	449	0	286.73	0.6652614	0.008	↓
17	tr|H0YAC1|	KLKB1	Plasma kallikrein (fragment)	76.773	686	0	148.39	0.6526857	0.005	↓
18	tr|Q5VY30|	RBP4	Retinol-binding protein 4, plasma, isoform CRA_b	22.974	199	0	94.794	0.630816	0.029	↓
19	tr|B4E1B2|	TF	cDNA FLJ53691, highly similar to serotransferrin	74.831	678	0	323.31	0.6304394	0.039	↓
20	sp|P05546|	SERPIND1	Heparin cofactor 2	57.07	499	0	130.1	0.6268114	0.004	↓
21	tr|Q53FV4|	LUM	Lumican variant (fragment)	38.413	338	0	21.207	0.6033161	0.001	↓
22	sp|A2NJV5|	IGKV3D-7	Immunoglobulin kappa variable 2-29	13.085	120	0	23.778	0.5528563	0.006	↓
23	sp|P06727|	APOA4	Apolipoprotein A-IV	45.398	396	0	261.29	0.5293484	0.030	↓
24	tr|A0A024R3E3|	APOA1	Apolipoprotein A-I, isoform CRA_a	30.777	267	0	323.31	0.4976017	0.015	↓
25	tr|X6RLJ0|	C1QA	Complement C1q subcomponent subunit A (fragment)	23.351	220	0	23.923	0.4945711	0.005	↑
26	tr|E9KL36|	TTR	Transthyretin	15.887	147	0	239.06	0.4477275	0.009	↑
27	tr|V9GYM3|	APOA2	Apolipoprotein A-II	14.914	133	0	54.723	0.4400852	0.008	↑
28	tr|D9YZU5|	HBB	Beta-globin	15.998	147	0	126.29	0.3773419	0.010	↑
29	tr|Q53H26|	TF	Transferrin variant (fragment)	77.079	698	0	81.553	0.3412472	0.021	↓
30	tr|A0A024R0T9|	APOC2	Apolipoprotein C-II isoform 1	11.284	101	0	30.162	0.2207795	0.008	↓
31	tr|A0A0G2JRQ6|	IGKV3D-7	Uncharacterized protein (fragment)	12.748	117	0.00303	11.523	Only detected in OSCC-LNM		↑
32	tr|A0A193CHR0|	ENSG00000223931	10E8 heavy-chain variable region (fragment)	14.429	131	0	18.246	Only detected in OSCC-LNM		↑

(Continued on the following page)

Table 1. Comparison of DEPs identified in SEs of the OSCC-LNM group versus the HC group (Cont'd)

Number	Accession number	Abbreviation	Full name	Molecular weight (kDa)	Sequence length	*Q* value[a]	Score[b]	OSCC-LNM/HC	*P* value	Expression
33	tr|B2R6V9|	F13A1	cDNA, FLJ93141, highly similar to Homo sapiens coagulation factor XIII, A1 polypeptide (F13A1), mRNA	83.24	732	0	17.861	Only detected in OSCC-LNM		↑
34	sp|P02741|	CRP	C-reactive protein	25.038	224	0	29.616	Only detected in OSCC-LNM		↑
35	sp|P0DOX4|	ENSG00000223931	Immunoglobulin epsilon heavy chain	60.322	547	0	35.141	Only detected in OSCC-LNM		↑
36	sp|P10720|	PF4V1	Platelet factor 4 variant	11.553	104	0	20.13	Only detected in HC		↓
37	tr|Q96SB0|	IGKV3D-7	Anti-streptococcal/anti-myosin immunoglobulin lambda light-chain variable region (fragment)	11.594	108	0	35.763	Only detected in HC		↓

[a]*Q* value, the probability that the protein is a false hit.
[b]Score, the sum of the scores of the individual peptides.

identified as associated with OSCC-LNM when compared with HC (Table 1), and a total of 28 DEPs with 15 upregulated proteins and 13 downregulated proteins were identified as associated with OSCC-LNM when the results were compared with OSCC-NLNM (Table 2). The DEPs were identified to be associated with OSCC-NLNM compared with HC, which are shown in Supplementary Table S2. A protein score >10 was exhibited in all the DEPs. The relative abundance of these proteins is listed in Tables 1 and 2. The fragments of four DEPs including the b-ion and y-ion series are shown in Supplementary Fig. S2.

To identify the OSCC-LNM–related physiologic processes involving the exosomal proteins, all identified proteins were then clustered into GO categories and KEGG signaling pathway enrichment analysis by applying bioinformatics tools.

(i) A total of nine significant enrichment results were obtained in GO classification analysis of DEPs in OSCC-LNM relative to HC (Fig. 2A1). When referring to biological processes, the proteins were mostly enriched in biological adhesive, cellular component organization, or biogenesis and cellular process. When referring to molecular functions and cellular component, the proteins were mostly enriched in the molecular carrier activity, structural molecule activity, transporter activity, macromolecular complex, and membrane-enclosed lumen. KEGG signaling pathway enrichment analysis revealed that most of the proteins were greatly responsible for graft-versus-host disease, platelet activation, and calcium signaling pathway (Fig. 2A2).

(ii) A total of one significant enrichment result was obtained in GO classification analysis of DEPs in OSCC-LNM relative to OSCC-NLNM (Fig. 2B1). When referring to biological processes, the proteins were enriched the most in the response to stimulus. KEGG signaling pathway enrichment analysis revealed that most of the proteins were greatly responsible for GPI anchor biosynthesis, gap junction, protein export, 2-oxocarboxylic acid metabolism, arginine biosynthesis, and chemokine signaling pathway (Fig. 2B2).

(iii) All 415 identified proteins went through the GO classification analysis. When referring to biological processes (Fig. 2C1), most of the proteins (>100) were involved in biological regulation, response to stimulus, metabolic process, extracellular region, extracellular region part, and binding. KEGG signaling pathway enrichment analysis revealed that most of the proteins were greatly responsible for complement and coagulation cascades and human papillomavirus infection (Fig. 2C2). Figure 2D also shows the hierarchical clustering representation of DEPs identified (Fig. 2D1: OSCC with LNM vs. HC; Fig. 2D2: OSCC with LNM vs. OSCC with NLNM) and the common DEPs identified between the OSCC with LNM versus HC group and the OSCC with LNM versus OSCC with NLNM group (Fig. 2E).

Verification of DEPs

PF4V1, ApoA1, CXCL7, and F13A1 were chosen for validation according to the bioinformatics analysis, available commercially antibodies and ELISA kits, and some evidence from previous research. Proteins were selected for the next step of validation based on three results. First, PF4V1 and CXCL7 participated in cytokine–cytokine receptor interaction and chemokine signaling pathway, and CXCL7 participated in transcriptional misregulation in cancer according to the bioinformatics analysis; moreover, chemokines had multiple functions such as chemotaxis, angiogenesis, tumorigenesis, and so on (27). Some publications have shown that these two proteins have been linked to various cancer-related pathways, including the PI3K–Akt signaling pathway, that were associated with tumor proliferation. Second, the expression of F13A1 was only detected in OSCC with LNM, and has been found to be associated with the risk of oral cancer (28). Third, ApoA1, which has been found to be associated with the risk of squamous cell carcinoma (29, 30), participated in PPAR signaling pathway and cAMP signaling pathway according to the bioinformatics analysis. PF4V1 was derived from CXCL4 and was found to have similar functions as CXCL4, so our study chose CXCL4 as the negative control in the validations.

ELISA, Western blot, and IHC validation. Western blot results indicated that the expression profiles of these three proteins in

Table 2. Comparison of the DEPs identified in SEs of the OSCC-LNM group versus the OSCC-NLNM group

Number	Accession number	Abbreviation	Full name	Molecular weight (kDa)	Sequence length	*Q* value[a]	Score[b]	OSCC-LNM/ OSCC-NLNM	*P* value	Expression
1	tr|A0A109PSY4|	IGKV3D-7	MS-A1 light-chain variable region (fragment)	11.376	106	0.000	49.696	3.874	0.0003564	↑
2	sp|P04040|	CAT	Catalase	59.755	527	0.000	20.916	2.503	0.0193373	↑
3	sp|P04275|	VWF	von Willebrand factor	309.26	2813	0.000	157.030	1.807	0.0184345	↑
4	tr|V9GYE7|	CFHR2	Complement factor H-related protein 2	28.912	254	0.000	24.488	1.762	0.0150898	↑
5	tr|B4DEF7|	HSPA5	cDNA FLJ60062, highly similar to 78 kDa glucose-regulated protein	30.419	278	0.000	29.640	1.702	0.0380467	↑
6	tr|A0A0 × 9V9C4|	ENSG00000223931	GCT-A8 heavy-chain variable region (fragment)	13.228	120	0.000	37.772	1.662	0.034641	↑
7	tr|B4DUV1|	FBLN1	Fibulin-1	70.154	641	0.000	153.190	1.648	0.0107605	↑
8	sp|P80108|	GPLD1	Phosphatidylinositol-glycan–specific phospholipase D	92.335	840	0.000	17.994	1.576	0.0105536	↑
9	tr|F2RM37|	F9	Coagulation factor IX	51.744	461	0.000	25.634	1.556	0.0244641	↑
10	sp|Q03591|	CFHR1	Complement factor H-related protein 1	37.65	330	0.000	117.800	1.552	0.0057128	↑
11	tr|Q68DS3|	CLEC3B	Uncharacterized protein DKFZp686H17246 (fragment)	14.708	133	0.000	71.101	1.517	0.0094758	↑
12	tr|Q6N030|	ENSG00000223931	Uncharacterized protein	57.019	518	0.000	323.310	0.595	0.0352034	↓
13	sp|P07360|	C8G	Complement component C8 gamma chain	22.277	202	0.000	121.680	0.587	0.0305837	↓
14	tr|A0A024R3E3|	APOA1	Apolipoprotein A-I, isoform CRA_a	30.777	267	0.000	323.310	0.539	0.0326735	↓
15	tr|A0A096LPE2|	SAA4	SAA2-SAA4 readthrough	23.353	208	0.000	33.364	0.519	0.0309882	↓
16	tr|D3JV41|	CXCL7	C-X-C motif chemokine (fragment)	13.708	126	0.000	156.490	0.340	0.0427637	↓
17	sp|P0DOX3|	ENSG00000223931	Immunoglobulin delta heavy chain	56.224	512	0.000	164.380	0.243	0.0377757	↓
18	tr|A0A140TA29|	C4B	Complement C4-B	187.66	1698	0.000	63.495	0.166	0.0162487	↓
19	sp|A0A0C4DH39|	ENSG00000223931	Immunoglobulin heavy variable 1–58	13.005	117	0.003	10.683	Only detected in OSCC-NLNM		↓
20	tr|A0A0F7T6Q1|	ENSG00000223931	IGHV1-2 protein (fragment)	11.911	105	0.000	78.857	Only detected in OSCC-NLNM		↓
21	sp|P10720|	PF4V1	Platelet factor 4 variant	11.553	104	0.000	20.130	Only detected in OSCC-NLNM		↓
22	tr|Q5NV70|	IGKV3D-7	V1-11 protein (fragment)	10.333	97	0.000	18.509	Only detected in OSCC-NLNM		↓
23	tr|Q8TCF0|	LBP	LBP protein	52.933	477	0.000	19.414	Only detected in OSCC-NLNM		↓
24	tr|Q96SA9|	IGKV3D-7	Human anti-streptococcal/ anti-myosin immunoglobulin kappa light-chain variable region (fragment)	11.52	107	0.000	12.329	Only detected in OSCC-NLNM		↓
25	tr|A0A0G2JRQ6|	IGKV3D-7	Uncharacterized protein (fragment)	12.748	117	0.003	11.523	Only detected in OSCC-LNM		↑
26	tr|B2R6V9|	F13A1	cDNA, FLJ93141, highly similar to Homo sapiens coagulation factor XIII, A1 polypeptide (F13A1), mRNA	83.24	732	0.000	17.861	Only detected in OSCC-LNM		↑
27	tr|B2RA39|	CFHR5	cDNA, FLJ94686, highly similar to Homo sapiens complement factor H-related 5 (CFHL5), mRNA	64.391	569	0.000	13.285	Only detected in OSCC-LNM		↑
28	tr|Q0ZCH1|	ENSG00000223931	Immunoglobulin heavy-chain variable region (fragment)	12.863	118	0.000	19.922	Only detected in OSCC-LNM		↑

[a]*Q* value, the probability that the protein is a false hit.
[b]Score, the sum of the scores of the individual peptides.

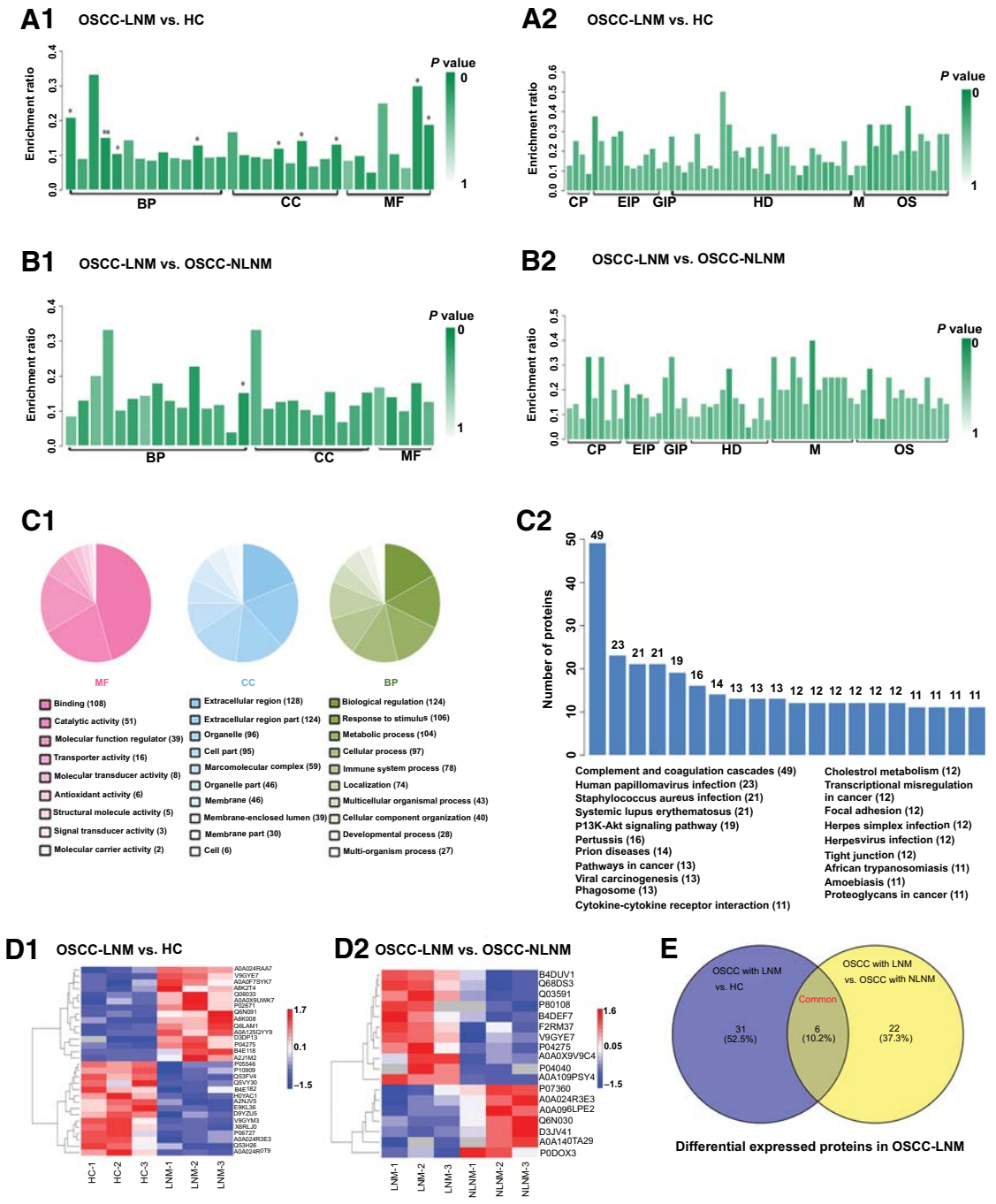

Figure 2.

Bioinformatics analysis of DEPs. GO classification analysis (**A1**) and KEGG analysis (**A2**) of DEPs in OSCC-LNM relative to HC. GO classification analysis (**B1**) and KEGG analysis (**B2**) of DEPs in OSCC-LNM relative to OSCC-NLNM. GO classification analysis (**C1**) and KEGG analysis (**C2**) of all identified proteins. **D,** The hierarchical clustering representation of DEPs identified (**D1**, OSCC with LNM vs. HC; **D2**, OSCC with LNM vs. OSCC with NLNM). **E,** Common DEPs identified between OSCC with LNM vs. HC group and OSCC with LNM vs. OSCC with NLNM group. BP, biological processes; CC, cellular component; CP, cellular processes; EIP, environmental information processing; GIP, genetic information processing; M, metabolism; MF, molecular functions; OS, organismal systems.

SEs were consistent with the proteomics results (Fig. 3). Similar results were obtained except for the missing detection of F13A1 in all serum samples. ELISA results were as follows (Supplementary Fig. S3): The expression level of CXCL7 was significantly reduced in serum or SEs from the OSCC-LNM group compared with OSCC-NLNM and HC groups ($P < 0.05$, Supplementary Fig. S3B1 and S3B2); the expression level of ApoA1 was significantly reduced in serum or SEs from OSCC-LNM and

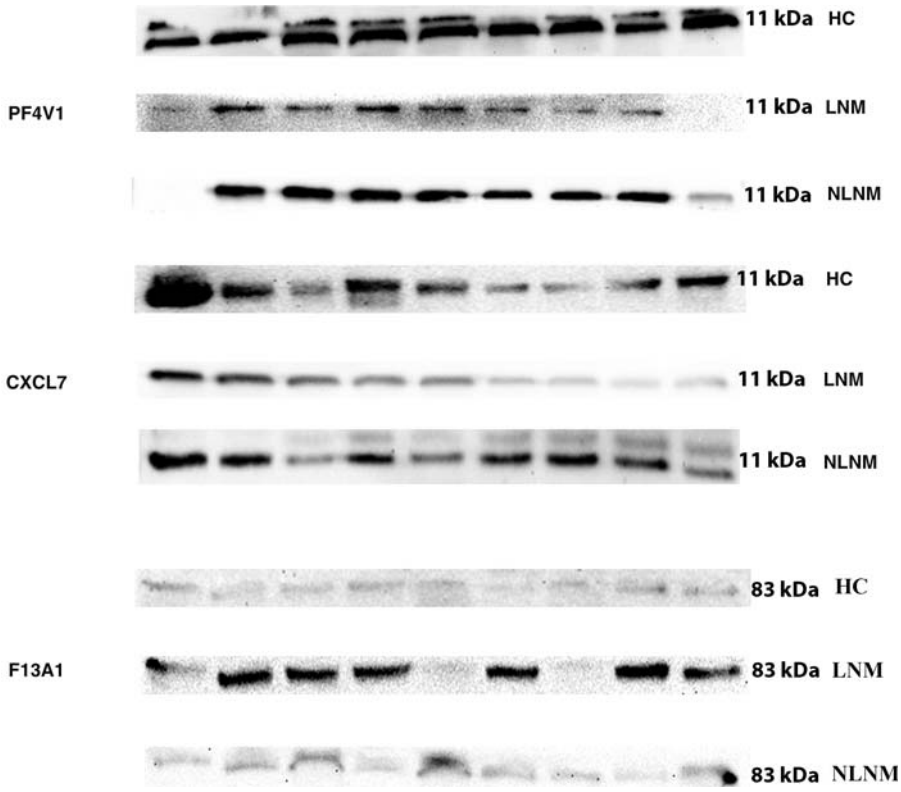

Figure 3.
Western blot validation of MS/MS data. Quantification of the expression levels of PF4V1, CXCL7, and F13A1 from Western blotting. "HC," "LNM," and "NLNM" represent the SEs of individual HCs, OSCC with LNM patients, and OSCC with NLNM patients, respectively.

OSCC-NLNM groups compared with the HC group ($P < 0.05$, Supplementary Fig. S3C1 and S3C2); and the expression levels of CXCL4 were not statistically different among the three groups ($P > 0.05$, Supplementary Fig. S3A1 and S3A2). These results were consistent with the proteomics results. IHC was used to examine the expression location of the identified proteins in tissues. For PF4V1 (Supplementary Fig. S4A1–S4A3) and CXCL7 (Supplementary Fig. S4B1 and S4B2), higher expression levels were present only in highly differentiated cancer cells than that in poorly differentiated cancer cells in cancer tissues. Stronger expression of F13A1 was observed in cancer tissues (Supplementary Fig. S4C1) when compared with that in the corresponding paracancerous tissues (Supplementary Fig. S4C2). There was no statistical difference in the expression of these three proteins in the LNM group and NLNM group of cancer tissue.

RT-PCR validation.

(i) mRNA expression levels in tissues were analyzed (Supplementary Fig. S3). Our findings showed a statistically significant increase of *ApoA1* expression in cancer tissue compared with paracancerous tissue (Supplementary Fig. S3C3), whereas there was no statistical difference in the LNM group and NLNM group of cancer tissue (Supplementary Fig. S3C4). Furthermore, the expression levels of *PF4V1*, *CXCL4*, *CXCL7*, and *F13A1* were not statistically different between cancer tissue and paracancerous tissue (Supplementary Fig. S3A3, S3B3, S3D1, and S3D3), and the same results were obtained between the LNM group and NLNM group of cancer tissue (Supplementary Fig. S3A4, S3B4, S3D2, and S3D4).

(ii) mRNA expression levels in serum were examined (Supplementary Fig. S5). Our finding showed a statistically significant increase for the expression of *ApoA1* in the OSCC with LNM group compared with the HC group, whereas there was no statistical difference in the OSCC with LNM group and OSCC with NLNM group in serum samples. Furthermore, the expressions of *PF4V1*, *CXCL4*, *CXCL7*, and *F13A1* were not statistically different among the LNM group, NLNM group, and HC group.

(iii) mRNA expression levels from the whole blood were examined (Supplementary Fig. S5). Our finding showed a statistically significant decrease for the expression of *ApoA1* and *F13A1* in the OSCC with LNM group and OSCC with NLNM group when compared with the HC group, whereas there was no statistical difference in the LNM group and NLNM group. Furthermore, the expression levels of *CXCL4* and *CXCL7* were significantly decreased in the OSCC with LNM group compared with the HC group, whereas there was no statistical difference between those in the LNM group and NLNM group or between the NLNM group and HC group. *PF4V1* expression level was significantly decreased in the OSCC with LNM group compared with the HC and OSCC with NLNM groups, whereas no statistical differences were found between the OSCC with NLNM group and HC group.

Clinicopathologic findings of patients with OSCC

When in comparison with all the clinicopathologic parameters, *ApoA1* was significantly higher in OSCC patients with smoking and drinking than in patients without smoking and

drinking (Supplementary Fig. S6C5), but no significant change in HCs with smoking and drinking than in HCs without smoking and drinking; *PF4V1* was significantly higher in well-differentiated squamous cell carcinoma patients than in low-differentiated squamous cell carcinoma patients (Supplementary Fig. S6A4). *PF4V1* was significantly lower in OSCC-LNM patients with $\geq$5 positive nodes than in patients with <5 positive nodes and 2 to 4 positive nodes in tissue specimen; F13A1 was significantly lower in OSCC-LNM patients with 1 to 2 positive nodes than in patients with 4 to 5 positive nodes in serum specimen (Supplementary Fig. S7). *ApoA1* and *PF4V1* had no statistical difference in other parameters. In terms of *CXCL4*, *CXCL7*, and *F13A1* expression, there was no statistically significant difference in any set of parameters (Supplementary Table S3). In terms of all validated DEP expression, there was no statistically significant difference among different age groups except for *F13A1* between $\leq$50 years and >50 years (Supplementary Table S4). Survival analysis provided by GEPIA showed that *ApoA1*, *CXCL7*, *PF4V1*, and *F13A1* had no connection with the overall survival of head and neck squamous cell carcinoma (Supplementary Fig. S8).

Combination biomarker models

Figure 4 shows the findings of various joint diagnoses, including the AUC, sensitivity, and specificity. Regarding *CXCL7*, the sensitivity and specificity of the combination of SE and whole blood specimen were higher than other combinations in differentiating OSCC with LNM from the OSCC with NLNM and HC groups (Fig. 4A); the sensitivity of the combination of serum, SE, and whole blood specimen and the specificity in serum were the highest in differentiating OSCC from the HC group (Fig. 4B). Regarding *ApoA1*, the sensitivity in whole blood specimen and the specificity in SE specimen were the highest; the sensitivity and specificity of the combination of serum, SE, and whole blood specimen were higher than other combinations and single specimens in differentiating OSCC from the HC group (Fig. 4D). Regarding whole blood specimen, the sensitivity and specificity of the combination of *PF4V1* and *ApoA1* were higher than other combinations and single biomarkers in differentiating OSCC with LNM from the OSCC with NLNM and HC groups (Fig. 4E). The sensitivity in whole blood specimen for single *CXCL7* and *ApoA1* and the specificity for single *PF4V1* and the combination of *PF4V1* and *ApoA1* were the highest in differentiating OSCC from the HC group (Fig. 4F). The sensitivity of *F13A1* in whole blood and the specificity of *ApoA1* were the highest in serum in differentiating OSCC with LNM from the OSCC with NLNM and HC groups. The sensitivity of *F13A1* in whole blood and the specificity of the combination of *F13A1* in whole blood and ApoA1 in serum were the highest in differentiating OSCC from the HC groups (Fig. 4H).

Discussion

Previous research has examined exosomes isolated from OSCC cells (3, 31, 32); however, there was no study measuring the differences in protein expression levels in SEs from serum using proteomics, especially with samples from OSCC with LNM patients. In this study, differences in protein levels were identified in the SEs of patients with OSCC with LNM relative to OSCC with NLNM patients and HCs on the basis of MS analysis, which identifies and quantifies the maximum protein levels precisely. There is a wide use for quantitative proteomics to examine the differences in global protein expression between HCs and disease samples to search for disease biomarker and target discovery (33). The label-free approaches used in our study were on the basis of one MS feature of abundance, for example, spectral and peptide count, chromatographic peak area, and height values (33, 34). Previous studies have found that label-free proteomics achieved statistically significant comprehensiveness and systematic analysis in DEP identification (35). The proteins identified in this study could be involved in different processes and functions that regulated the metastasis, occurrence, and progression of OSCC with LNM. It has been shown that SEs of colorectal cancer patients had a significant effect on accelerating the tumor invasion, which elucidated the pathophysiologic functions of tumor-derived exosomes and aided in the development of tumor diagnostics and therapeutics (36).

The exosomes secreted into the blood circulation of OSCC with LNM patients might establish the premetastatic niche by influencing tumor migration. This study revealed that several typical proteins involved in the establishment for the premetastatic niche of cancer had differential expression levels in the SEs of patients with OSCC with LNM.

Our findings show that two chemokine factors, CXCL7 and PF4V1, had decreased or absent expression in OSCC with LNM group; besides, it turned out that there was a very strong correlation between PF4V1 and the differentiation degree of OSCC and the number of positive nodes of OSCC-LNM. These two factors played a critical role in the homing of metastatic tumor cells. PF4V1 has recently been considered as a naturally nonallelic gene variant and was derived from CXCL4, which was identified to have no relationship with OSCC with LNM in this study (37). Some research has shown that PF4V1 could be cloned, and the purified recombinant protein was found to have a more active and stronger role in preventing the tumor metastases to the lymph nodes by inhibiting tumor lymphangiogenesis, cell migration, tumor growth, angiogenesis, and mobilizing bone marrow–derived cells relative to CXCL4 (38, 39). Our study showed that the deletion of PF4V1 was found in the OSCC with LNM group compared with the other two controls, implying that the antitumor effect of PF4V1 was ineffective with a high lymph node metastatic rate. Therefore, in this study, it was speculated that the absence of SE PF4V1 may induce the development of OSCC under the possible mechanisms as follows (38–41): (i) inducing the formation of prelymph node metastatic niche by hindering immune effector cells reaching the tumor site; (ii) promoting tumor angiogenesis; (iii) regulating the function and differentiation of immune effector cells; (iv) promoting tumor cell migration and invasion, and the remodeling of ECM and tumor vessel basement membrane. Furthermore, it was found that human PF4V1 expression was induced in human osteosarcoma cells and detected in leiomyosarcoma, liposarcoma, and colorectal carcinoma tissue samples (42), whereas PF4V1 had weak to negative expression in squamous cell carcinoma of the exophages (43). Biological effects of PF4V1 on leukocytes included chemotaxis of dendritic cells and activated T-cell migration. CXCR3 has recently been identified as the functional receptor for PF4V1 in humans, which was shown to functionally participate in the angiostatic and chemotactic

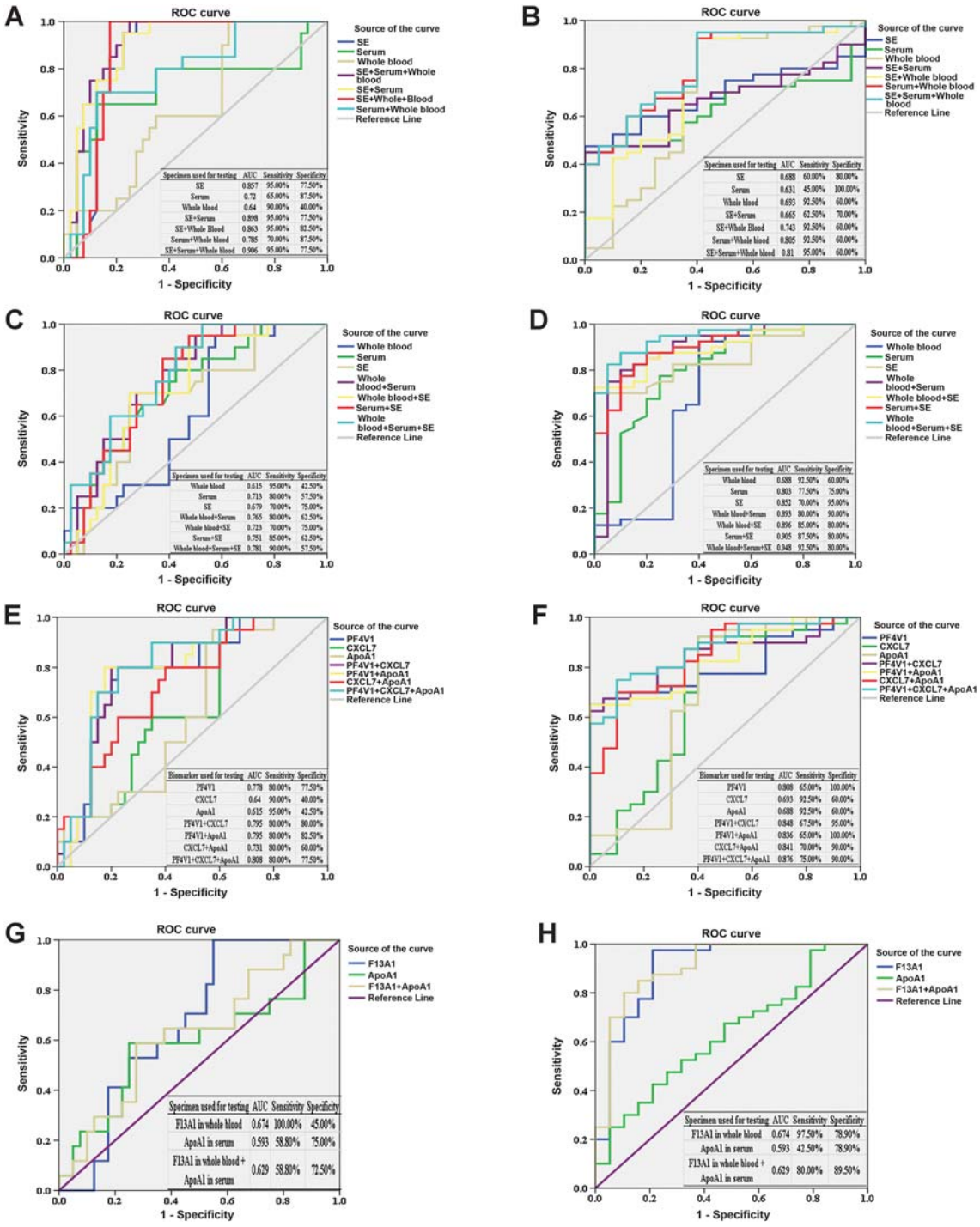

Figure 4.

ROC analysis of the newly developed biomarker panels. ROC curves of CXCL7 and ApoA1 expression levels in SE, serum, whole blood, and the combinations of the three specimens are shown for differentiating OSCC with LNM vs. OSCC with NLNM and HC group (**A** for CXCL7, **C** for ApoA1), and OSCC vs. HC groups (**B** for CXCL7, **D** for ApoA1). ROC curves of PF4V1, CXCL7, ApoA1, and the combinations of the three novel biomarkers are shown for differentiating OSCC with LNM vs. OSCC with NLNM and HC group (**E**), and OSCC vs. HC groups (**F**). ROC curves of F13A1 in whole blood, ApoA1 in serum, and the combinations are shown for differentiating OSCC with LNM vs. OSCC with NLNM and HC group (**G**), and OSCC vs. HC groups (**H**).

activities of PF4V1. Most interestingly, our findings also indicated that another chemokine, CXCL7, had a significantly decreased expression level in the OSCC with LNM group than that in the OSCC with NLNM group. CXCL7, also known as neutrophil-activating peptide-2, has previously been reported to be used for diagnosis of tumors (44–46). It has been found that the CXCL7 and CXCL4 genes were inextricably related (separated by 7 kb) and formed a complex that appeared in the process of megakaryocyte differentiation. It was an exciting finding that both CXCL7 and PF4V1 protein levels decreased in the OSCC with LNM group, which further corroborated that CXC chemokines were involved in promoting angiogenesis, occurrence, and metastasis of tumor by increasing the expression levels of lymph angiogenesis factors. Remarkably, there was no significant difference in CXCL7 protein expression between the NLNM group and HC group. Based on the analyses above, we could draw a conclusion that CXCL7 was a useful biomarker in differentiating the LNM group from the NLNM group but was not useful in identifying the OSCC group and HC group. Based on KEGG pathway and interaction network analysis, PF4V1 combined with CXCL7 also plays an important role in promoting tumor cell metastasis via the activation of cytokine–cytokine receptor interaction and the chemokine signaling pathway. Further evaluations of PF4V1 and CXCL7 structures and functions are necessary to point to a new direction for their roles in OSCC with LNM. A lot of studies have reported that exosomal-mediated cellular adhesion in tumor cell lines drives the adhesion process (36).

F13A1 was only detected in the OSCC with LNM group in our study, implying that F13A1 was relevant to lymphatic metastasis; moreover, F13A1 was significantly lower in OSCC-LNM patients with 1 to 2 positive nodes than in patients with 4 to 5 positive nodes. A previous study demonstrated that *F13A1* genotypes were identified to have a strong correlation with OSCC risk; furthermore, *F13A1* gene polymorphism led to the generation of a fibrous network with thinner fibers and smaller pores that contributed to the acceleration of the initial tumor cell proliferation (28). Beyond that, however, there are few reports on its relationship to tumors. We would explore the mechanism of F13A1 with OSCC as our next step.

ApoA1 constituted about 70% of high-density lipoprotein particles. Several reported investigations revealed the changes of the expression level of serum lipids and lipoprotein in cancer patients, and some of those changes were in connection with cancer progression. The reported serum level ApoA1 had significant changes in patients with bladder cancer (47), esophageal squamous cell carcinoma (30), cervical squamous cell carcinoma (29), and ovarian cancer (48). We observed that the ApoA1 level in SEs was significantly lower in OSCC with LNM patients than that in OSCC with NLNM patients and HCs, which was in agreement with previous reports. Low serum levels of pretreatment ApoA1 in nasopharyngeal carcinoma patients were associated with an increased risk of distant metastasis. A recent study revealed that ApoA1 had an important role in tumor invasion and metastasis in colonic adenocarcinoma (49). Our finding implies that low levels of ApoA1 could indirectly promote tumor lymph node metastasis in OSCC patients. Intriguingly, ApoA1 was significantly higher in OSCC patients with smoking and drinking than in patients without smoking and drinking in comparison with all the clinicopathologic parameters. Moreover, the expression of ApoA1 had no significant change in HC with smoking and drinking than in HC without smoking and drinking in this study. Therefore, ApoA1 may be one of the potential biomarkers for OSCC in SEs and serum samples, especially for the smokers and alcohol drinkers.

Those results verified by RT-PCR and IHC, however, did not correspond to the serum and SE verification. Moreover, survival analysis provided by GEPIA showed that *ApoA1*, *CXCL7*, *PF4V1*, and *F13A1* had no connection with the overall survival of head and neck squamous cell carcinoma. Because of common clinical misdiagnosis, the proposed joint applications of biomarkers were recommended in order to improve the diagnostic accuracy of OSCC-LNM as required. A panel of proteins relevant to OSCC with LNM was observed in this study, and the results of the ROC analysis indicated that the combinations of the new panels were obviously superior to single biomarker for the diagnosis of OSCC with LNM.

In conclusion, our study showed that ApoA1, CXCL7, PF4V1, and F13A1 have certain potential application values as novel predictive circulating biomarkers for OSCC with LNM but are not useful in prognosis. Moreover, the combined applications of these biomarkers are recommended in order to reduce the clinical misdiagnosis of OSCC-LNM. The limitation to mention was that a relatively small sample size existed in the validation phase. Well-designed and large-sample studies are needed.

Disclosure of Potential Conflicts of Interest

No potential conflicts of interest were disclosed.

Authors' Contributions

Conception and design: C. Li, Y. Zhou, X. Su, H. Qin, S. Huang, X. Huang, N. Zhou
Development of methodology: Y. Zhou, X. Su
Acquisition of data (provided animals, acquired and managed patients, provided facilities, etc.): J. Liu, X. Su, H. Qin
Analysis and interpretation of data (e.g., statistical analysis, biostatistics, computational analysis): C. Li, Y. Zhou, J. Liu, S. Huang
Writing, review, and/or revision of the manuscript: C. Li, X. Huang, N. Zhou
Administrative, technical, or material support (i.e., reporting or organizing data, constructing databases): X. Huang
Study supervision: C. Li

Acknowledgments

The authors thank all of the study participants.

This work is supported by grants from the Guangxi Natural Science Foundation (Grant No. 2018GXNSFAA138003), Youth Science Foundation of Guangxi Medical University (Grant No. GXMUYSF201702), and Middle-aged and Young Teacher's Basic Ability Promotion Project of Guangxi (Grant No. 2018KY0129).

The costs of publication of this article were defrayed in part by the payment of page charges. This article must therefore be hereby marked *advertisement* in accordance with 18 U.S.C. Section 1734 solely to indicate this fact.

Received October 18, 2018; revised January 27, 2019; accepted July 23, 2019; published first July 26, 2019.

References

1. Kang H, Kiess A, Chung CH. Emerging biomarkers in head and neck cancer in the era of genomics. Nat Rev Clin Oncol 2014;12:11–26.
2. Rivera C. Essentials of oral cancer. Int J Clin Exp Pathol 2015;8:11884–94.
3. Li L, Li C, Wang S, Wang Z, Jiang J, Wang W, et al. Exosomes derived from hypoxic oral squamous cell carcinoma cells deliver miR-21 to normoxic cells to elicit a prometastatic phenotype. Cancer Res 2016;76: 1770–80.
4. Hanahan D. Weinberg RA. Hallmarks of cancer: the next generation. Cell 2011;144:646–74.
5. Giancotti FG. Mechanisms governing metastatic dormancy and reactivation. Cell 2013;155:750–64.
6. EL Andaloussi S1, Mäger I, Breakefield XO, Wood MJ. Extracellular vesicles: biology and emerging therapeutic opportunities. Nat Rev Drug Discov 2013;12:347–57.
7. Melo SA, Luecke LB, Kahlert C, Fernandez AF, Gammon ST, Kaye J, et al. Glypican-1 identifies cancer exosomes and detects early pancreatic cancer. Nature 2015;523:177–82.
8. Tkach M, Thery C. Communication by extracellular vesicles: where we are and where we need to go. Cell 2016;164:1226–32.
9. Choi DS1, Yang JS, Choi EJ, Jang SC, Park S, Kim OY, et al. The protein interaction network of extracellular vesicles derived from human colorectal cancer cells. J Proteome Res 2012;11:1144–51.
10. Colombo M, Raposo G, Thery C. Biogenesis, secretion, and intercellular interactions of exosomes and other extracellular vesicles. Annu Rev Cell Dev Biol 2014;30:255–89.
11. Liu Y, Gu Y, Han Y, Zhang Q, Jiang Z, Zhang X, et al. Tumor exosomal RNAs promote lung pre-metastatic niche formation by activating alveolar epithelial TLR3 to recruit neutrophils. Cancer Cell 2016;30:243–56.
12. Peinado H, Alečković M, Lavotshkin S, Matei I, Costa-Silva B, Moreno-Bueno G, et al. Melanoma exosomes educate bone marrow progenitor cells toward a pro-metastatic phenotype through MET. Nat Med 2012;18:883–91.
13. Costa-Silva B, Aiello NM, Ocean AJ, Singh S, Zhang H, Thakur BK, et al. Pancreatic cancer exosomes initiate pre-metastatic niche formation in the liver. Nat Cell Biol 2015;17:816–26.
14. Hong BS, Cho JH, Kim H, Choi EJ, Rho S, Kim J, et al. Colorectal cancer cell-derived microvesicles are enriched in cell cycle-related mRNAs that promote proliferation of endothelial cells. BMC Genomics 2009;10:556.
15. Altevogt P, Bretz NP, Ridinger J, Utikal J, Umansky V. Novel insights into exosome-induced, tumor-associated inflammation and immunomodulation. Semin Cancer Biol 2014;28:51–7.
16. Whiteside TL. Immune modulation of T-cell and NK (natural killer) cell activities by TEXs (tumour-derived exosomes). Biochem Soc Trans 2013; 41:245–51.
17. Saleem SN, Abdel-Mageed AB. Tumor-derived exosomes in oncogenic reprogramming and cancer progression. Cell Mol Life Sci 2015;72:1–10.
18. Ye SB, Li ZL, Luo DH, Huang BJ, Chen YS, Zhang XS, et al. Tumor-derived exosomes promote tumor progression and T-cell dysfunction through the regulation of enriched exosomal microRNAs in human nasopharyngeal carcinoma. Oncotarget 2014;5:5439–52.
19. Zhao L, Liu W, Xiao J, Cao B. The role of exosomes and "exosomal shuttle microRNA" in tumorigenesis and drug resistance. Cancer Lett 2015;356: 339–46.
20. Kahlert C, Kalluri R. Exosomes in tumor microenvironment influence cancer progression and metastasis. J Mol Med (Berl) 2013;91:431–7.
21. Yang C, Robbins PD. The roles of tumor-derived exosomes in cancer pathogenesis. Clin Dev Immunol 2011;2011:842849.
22. Mrizak D, Martin N, Barjon C, Jimenez-Pailhes AS, Mustapha R, Niki T, et al. Effect of nasopharyngeal carcinoma-derived exosomes on human regulatory T cells. J Natl Cancer Inst 2015;107:363.
23. Livak KJ, Schmittgen TD. Analysis of relative gene expression data using real-time quantitative PCR and the 2(-Delta Delta C(T)) method. Methods 2001;25:402–8.
24. Lee EJ, Park JS, Lee YY, Kim DY, Kang JL, Kim HS. Anti-inflammatory and anti-oxidant mechanisms of an MMP-8 inhibitor in lipoteichoic acid-stimulated rat primary astrocytes: involvement of NF-κB, Nrf2, and PPAR-γ signaling pathways. J Neuroinflammation 2018;23;15:326.
25. DeLong ER, DeLong DM, Clarke-Pearson DL. Comparing the areas under two or more correlated receiver operating characteristic curves: a nonparametric approach. Biometrics 1988;44:837–45.
26. Liu X, Zheng W, Wang W, Shen H, Liu L, Lou W, et al. A new panel of pancreatic cancer biomarkers discovered using a mass spectrometry-based pipeline. Br J Cancer 2018;118:e15.
27. Moser B, Wolf M, Walz A, Loetscher P. Chemokines: multiple levels of leukocyte migration control. Trends Immunol 2004;25:75–84.
28. Vylliotis A, Yapijakis C, Nkenke E, Nisyrios T, Avgoustidis D, Adamopoulou M, et al. Effect of thrombosis-related gene polymorphisms upon oral cancer: a regression analysis. Anticancer Res 2013;33:4033–9.
29. Guo X, Hao Y, Kamilijiang M, Hasimu A, Yuan J, Wu G, et al. Potential predictive plasma biomarkers for cervical cancer by 2D-DIGE proteomics and Ingenuity Pathway Analysis. Tumour Biol 2015;36:1711–20.
30. Wang XP, Li XH, Zhang L, Lin JH, Huang H, Kang T, et al. High level of serum apolipoprotein A-I is a favorable prognostic factor for overall survival in esophageal squamous cell carcinoma. BMC Cancer 2016;16: 516.
31. Sento S, Sasabe E, Yamamoto T. Application of a persistent heparin treatment inhibits the malignant potential of oral squamous carcinoma cells induced by tumor cell-derived exosomes. PLoS One 2016;11: e0148454.
32. Sakha S, Muramatsu T, Ueda K, Inazawa J. Exosomal microRNA miR-1246 induces cell motility and invasion through the regulation of DENND2D in oral squamous cell carcinoma. Sci Rep 2016;6:38750.
33. Griffin NM, Yu J, Long F, Oh P, Shore S, Li Y, et al. Label-free, normalized quantification of complex mass spectrometry data for proteomic analysis. Nat Biotechnol 2010;28:83–9.
34. Cox J, Mann M. MaxQuant enables high peptide identification rates, individualized ppb-range mass accuracies and proteome-wide protein quantification. Nat Biotechnol 2008;26:1367–72.
35. Wis´niewski JR, Zougman A, Nagaraj N, Mann M. Universal sample preparation method for proteome analysis. Nat Methods 2009;6:359–62.
36. Chen Y, Xie Y, Xu L, Zhan S, Xiao Y, Gao Y, et al. Protein content and functional characteristics of serum-purified exosomes from patients with colorectal cancer revealed by quantitative proteomics. Int J Cancer 2017; 140:900–13.
37. Dinsart C, Pervolaraki K, Stroh-Dege A, Lavie M, Ronsse I, Rommelaere J, et al. Recombinant parvoviruses armed to deliver CXCL4L1 and CXCL10 are impaired in their antiangiogenic and antitumoral effects in a Kaposi sarcoma tumor model due to the chemokines' interference with the virus cycle. Hum Gene Ther 2017;28:295–306.
38. Struyf S, Burdick MD, Peeters E, Van den Broeck K, Dillen C, Proost P, et al. Platelet factor-4 variant chemokine CXCL4L1 inhibits melanoma and lung carcinoma growth and metastasis by preventing angiogenesis. Cancer Res 2007;67:5940–8.
39. Prats AC, Van den Berghe L, Rayssac A, Ainaoui N, Morfoisse F, Pujol F, et al. CXCL4L1-fibstatin cooperation inhibits tumor angiogenesis, lymphangiogenesis and metastasis. Microvasc Res 2013;89:25–33.
40. Vandercappellen J, Van Damme J, Struyf S. The role of the CXC chemokines platelet factor-4 (CXCL4/PF-4) and its variant (CXCL4L1/PF-4var) in inflammation, angiogenesis and cancer. Cytokine Growth Factor Rev 2011;22:1–18.
41. Billottet C, Quemener C, Bikfalvi A. CXCR3, a double-edged sword in tumor progression and angiogenesis. Biochim Biophys Acta 2013;1836: 287–95.
42. Vandercappellen J, Noppen S, Verbeke H, Put W, Conings R, Gouwy M, et al. Stimulation of angiostatic platelet factor-4 variant (CXCL4L1/PF-4var) versus inhibition of angiogenic granulocyte chemotactic protein-2 (CXCL6/GCP-2) in normal and tumoral mesenchymal cells. J Leukoc Biol 2007;82:1519–30.
43. Verbeke H, De Hertogh G, Li S, Vandercappellen J, Noppen S, Schutyser E, et al. Expression of angiostatic platelet factor-4var/CXCL4L1 counterbalances angiogenic impulses of vascular endothelial growth factor, interleukin-8/CXCL8, and stromal cell-derived factor 1/CXCL12 in esophageal and colorectal cancer. Hum Pathol 2010;41:990–1001.
44. Du Q, Li E, Liu Y, Xie W, Huang C, Song J, et al. CTAPIII/CXCL7: a novel biomarker for early diagnosis of lung cancer. Cancer Med 2018;7: 325–35.
45. Kinouchi T, Uemura M, Wang C, Ishizuya Y, Yamamoto Y, Hayashi T, et al. Expression level of CXCL7 in peripheral blood cells is a potential biomarker for the diagnosis of renal cell carcinoma. Cancer Sci 2017;108: 2495–502.

46. Guo Q, Jian Z, Jia B, Chang L. CXCL7 promotes proliferation and invasion of cholangiocarcinoma cells. Oncol Rep 2017;37: 1114–22.
47. Chen YT, Chen CL, Chen HW, Chung T, Wu CC, Chen CD, et al. Discovery of novel bladder cancer biomarkers by comparative urine proteomics using iTRAQ technology. J Proteome Res 2010;9:5803–15.
48. Fung ET. A recipe for proteomics diagnostic test development: the OVA1 test, from biomarker discovery to FDA clearance. Clin Chem 2010;56: 327–9.
49. Tachibana M, Ohkura Y, Kobayashi Y, Sakamoto H, Tanaka Y, Watanabe J, et al. Expression of apolipoprotein A1 in colonic adenocarcinoma. Anticancer Res 2003;23:4161–7.

Potential Markers from Serum-Purified Exosomes for Detecting Oral Squamous Cell Carcinoma Metastasis

Cuiping Li, Yang Zhou, Junjun Liu, et al.

Cancer Epidemiol Biomarkers Prev Published OnlineFirst July 26, 2019.